Optical Detection of Phase-Resolved Ferromagnetic Resonance in Epitaxial FeCo Thin Films

Yi Li[1,2], Fanlong Zeng[3], Hilal Saglam[2,4], Joseph Sklenar[2,5], John E. Pearson[2], Thomas Sebastian[6], Yizheng Wu[3], Axel Hoffmann[2], *Fellow, IEEE*, and Wei Zhang[1,2]

[1]Department of Physics, Oakland University, Rochester, MI 48309 USA
[2]Materials Science Division, Argonne National Laboratory, Argonne, IL 60439 USA
[3]Department of Physics, Fudan University, Shanghai 200433, China
[4]Department of Physics, Illinois Institute of Technology, Chicago, IL 60616 USA
[5]Department of Physics, University of Illinois at Urbana–Champaign, Champaign, IL 61801 USA
[6]THATec Innovation GmbH, 01328 Dresden, Germany

We report phased-resolved ferromagnetic resonance (FMR) measurements in an epitaxial $Fe_{50}Co_{50}$ thin film using a heterodyne, optical detection method. We track the evolution of the precessional phase across the saturated and unsaturated regimes along the FeCo hard axis. For the two regimes, opposite phase evolutions with frequency are observed, which coincide with the negative effective field dependence on the biasing field for the unsaturated modes. In addition, a nonzero phase advance between 0.2 and 0.4 rad is found for the saturated with respect to the unsaturated modes, which indicates an incomplete spatial overlap of the two modes in the film caused by surface pinning effect. The optical method has the advantage of resolving both the spatial and phase information in FMR measurements, which will be closely relevant and adaptable to epitaxial samples with multiple anisotropy axes, and for both flip-chip-based continuous films and spin-torque-based nano-devices.

Index Terms—**Epitaxial films, ferromagnetic resonance (FMR), optical detection.**

I. Introduction

PRACTICAL applications of magnetic materials such as magnetic recording, sensors, and magnetic textures call for understanding and engineering of the magnetization states at zero or low biasing fields [1]. Currently, most functional designs of magnetic devices are still based on the macrospin model. This is a reasonable approximation in most polycrystalline magnetic films due to the negligible "internal field" averaged out by the random magnetocrystalline anisotropy and the ease to saturate the magnetization with small biasing fields. For an epitaxial system with a strong internal magnetocrystalline anisotropy, however, it is much more difficult to saturate the film and the macrospin model may fail to correctly predict either the static [2] or dynamic magnetic characteristics [3]. For example, the static magnetization reversal is usually achieved by domain wall processes among energy equivalent, degenerated spin axes [4]–[8], and the dynamical response is often governed by complex spin-wave modes [9]. Therefore, it is necessary to examine the validity of the macrospin assumption, especially in epitaxial films and at fields that are far lower than the anisotropy fields of the devices.

Here, we conduct phase-resolved ferromagnetic resonance (FMR) measurements of an epitaxial $Fe_{50}Co_{50}$ thin film. In particular, we are interested in the low-field, *unsaturated* FMR modes in comparison to their *saturated* counterparts at the same frequency along the hard axis, which could provide additional information besides the resonance field and magnetocrystalline anisotropy [10], [11]. We use a locally probed optical method (in Section II) for detecting FMR with the ability to also resolve the spin precessional phase (in Section III). For the two modes, we observe linear but opposite frequency dependence of the precessional phases relative to the microwave frequency, which is attributed to the reversed effective field dependence on the biasing field for the unsaturated modes. In addition, we identify a small but non-zero phase offset between the two modes, around 0.2 and 0.4 rad, indicating a spatial separation of the saturated and unsaturated modes in the film caused by the surface pinning effect to the FMR excitation.

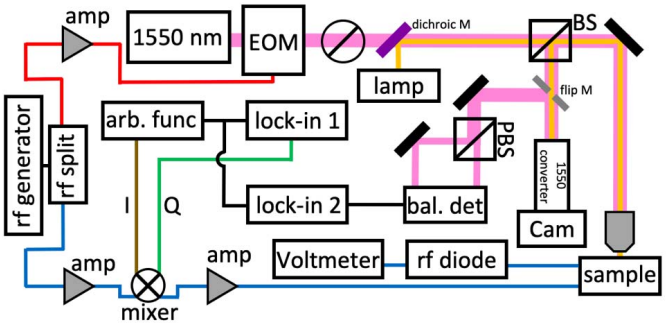

Fig. 1. Schematics of the heterodyne magneto-optic Kerr effect (MOKE) measurements. After the RF splitter, the optical path (top) contains amplifier, 1550 nm infrared laser module, electro-optic modulator (EOM), polarizer, beam splitter (BS), and focusing lens; the electrical path (bottom) contains amplifier, mixer, RF diode, and voltmeter. (PBS = polarizing beam splitter, Cam = camera, bal.det = balancing detector, arb. func = arbitrary waveform generator.)

II. Optical Method

The FMR signals are detected optically by polar magnetooptic Kerr effect which stroboscopically measures the

Manuscript received November 1, 2018; accepted January 10, 2019. Date of publication February 25, 2019; date of current version June 20, 2019. Corresponding authors: Y. Wu, A. Hoffmann, and W. Zhang (e-mail: wuyizheng@fudan.edu.cn; hoffmann@anl.gov; weizhang@oakland.edu).

Color versions of one or more of the figures in this paper are available online at http://ieeexplore.ieee.org.

Digital Object Identifier 10.1109/TMAG.2019.2893819

out-of-plane component of precessing magnetization. A heterodyne method is adopted to enable precessional phase extraction [12] using a setup illustrated in Fig. 1. A single microwave source (BNC-845, Berkeley-Nucleonics) was used to simultaneously modulate the detecting laser light (optical path) and drive the FMR of the sample (electrical path). On the optical path, we used a 1550 nm pigtail fiber laser (Thorlabs LPSC-1550-FC) outputting continuous-wave light with adjustable power up to 5 mW. The laser light was modulated at the microwave source frequency using an electro-optic modulator (EOM, Optilab IM-1550-12-PM). For optimal laser power, we also used a laser amplifier (Thorlabs EDFA100S) and a fiber-based polarization controller (Thorlabs FPC032) in front of the EOM. The modulated laser light was then converted to free space and polarized before focused onto the sample surface. The focused light spot is set to $\sim$40 μm in this paper. The electric path of the measurement is similar to the conventional flip-chip FMR using an RF diode (Mini-Circuits, ZX47-40LN-S+) and a voltmeter (Keithley 2000). For the given spot size and laser power, the laser heating effect is negligible as monitored by the device resistance.

For a heterodyne detection, the microwave signal along the electrical path was mixed (Pasternack PE86X9000) with a low-frequency (100 kHz) signal provided by a waveform generator (Keysight 33621A) and a synchronized, lock-in amplifier (Stanford Research SR830). The voltage amplitude, offset, and phase for the respective "I" and "Q" channels were optimized to ensure the power of the upper sideband of the microwave signal (which was subsequently used for FMR excitation) exceeds those of the central and lower sideband. In this experiment, we used 430 mVpp outputs from the waveform generator and the lock-in, and a 98° phase difference between the "I" and "Q" for optimal sideband performance, monitored simultaneously by a real-time spectrum analyzer (RTSA-7550, Berkeley-Nucleonics) and a 6 GHz digital oscilloscope (Keysight DSOX6002A).

The resultant, out-of-plane, dynamical Kerr response of the sample was then probed by the modulated light, sent into a balancing detector (Thorlabs PDB210C) after polarization splitting (Thorlabs PBS254), and analyzed by another lock-in amplifier (Stanford Research SR830). A series of RF amplifiers (Mini-circuits, ZX60-8008E-S+, ZX60-14012L-S+) and programmable attenuators (RUDAT-13G-60) were also used for signal strength adjustments as needed. The device synchronization and software control were conveniently achieved by customized modules and central programming interfaces developed by THATec Innovation GmbH [13].

III. Results and Discussion

Single-crystalline body center-cubic FeCo(10 nm) film was prepared on a two-side-polished MgO(001) single-crystal substrate by molecular beam epitaxy in an ultrahigh vacuum chamber [14]. The high-quality surface of the FeCo film was confirmed by *in situ* reflection high-energy electron diffraction patterns. Angular-dependent inductive FMR measurements in the saturated regime, reported elsewhere [15], show that the FeCo films have in-plane, fourfold magnetocrystalline anisotropy with the easy axis along FeCo-⟨110⟩ direction. We obtained a magnetization of 24.7 kG, an in-plane cubic anisotropy field of 480 G, and a uniaxial anisotropy field of 120 G [15]. Because the inductive FMR does not resolve the precessional phase of the magnetization dynamics, we hereby use the optical FMR detection and focus on the unsaturated modes in comparison to the saturated modes. The sample is flipped on a coplanar waveguide and the laser is introduced from the back side of the substrate. The dc bias magnetic field H_B is applied along the FeCo-[110] hard axis where the uniaxial anisotropy also stays.

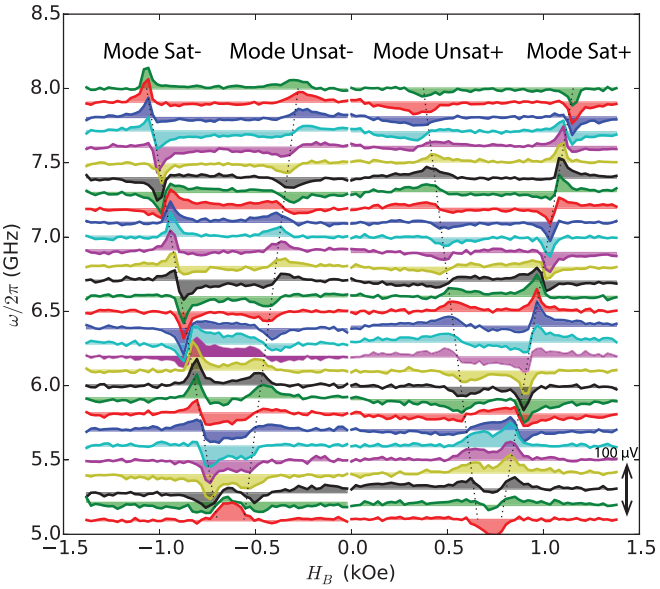

Fig. 2. Optically measured FMR traces of $Co_{50}Fe_{50}$ (10 nm) continuous films measured at 5.1–8.0 GHz frequency range. The biasing field is applied along FeCo-[110] hard axis and crosses the saturated and unsaturated regimes.

Fig. 2 shows the optically measured resonance lineshapes as a function of H_B, with the microwave frequency set between 5.1 and 8.0 GHz. For both positive and negative H_B, we can observe the saturated and unsaturated modes denoted by the black-dotted curves. They have the opposite frequency dependence on the resonance field. Extrapolating the spectra pair versus the frequency yields a crossing point at $H_B = \pm 660$ Oe, which is similar to the sum of the cubic and uniaxial anisotropy field as 600 Oe. A finite remnant resonance frequency $\omega_r/2\pi = 5$ GHz at the crossing point is due to the imperfection from the macrospin such as grain inhomogeneity, surface pinning, and field misalignment.

To extract the frequency-dependent phase of spin precession, each resonance line shape is fitted to a complex Lorentzian function with a mixing phase ϕ to the microwave field

$$V_D = \mathrm{Re}\left[\frac{Ae^{i\phi}}{(H_B - H_{\mathrm{res}}) + i\,\Delta H_{1/2}/2}\right] \tag{1}$$

where H_{res} is the resonance field, $\Delta H_{1/2}$ is the full-width-half-maximum linewidth, A is the amplitude, and ϕ represents the precessional phase of the magnetization plus a constant delay of microwave between the electrical path and the optical path. In addition, it is noted that the denominator of (1) introduces

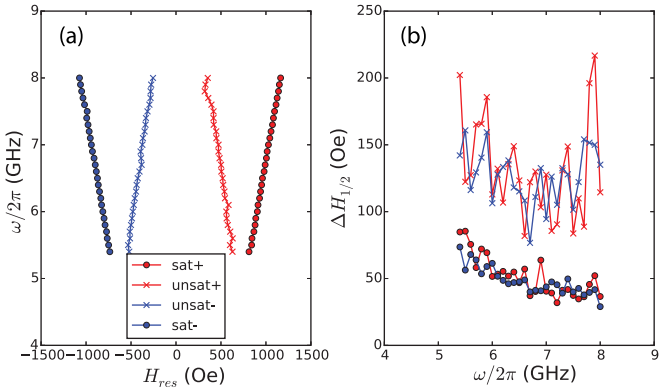

Fig. 3. Extracted (a) $H_{\rm res}$ and (b) $\Delta H_{1/2}$ from Fig. 2 between 5.4 and 8.0 GHz, where the data with lower frequencies cannot get good fits.

an additional phase of $-\pi$ when H_B goes from below to above $H_{\rm res}$. This will become different for the unsaturated mode, which will be discussed later. The extracted $H_{\rm res}$ and $\Delta H_{1/2}$ for different frequencies are summarized in Fig. 3(a) and (b). The $\Delta H_{1/2}$ has a non-monotonic behavior because the magnetization is not fully saturated. Also, the much larger $\Delta H_{1/2}$ of the unsaturated mode than the saturated modes is due to the significant deviation of the magnetization from the biasing field at low fields.

We emphasize the ability to reveal the phase information ϕ from the optical FMR measurements. Fig. 4(a) and (b) shows the extracted ϕ as a function of frequency for the saturated and unsaturated modes, respectively. Three observations are made from the phase measurements:

A. For Both Modes, ϕ Evolves Linearly as a Function of ω With the Same Slope

This is due to the phase accumulation from the finite path difference ΔL between the optical and electrical paths [12], with a dependence of $\delta\phi = \omega\Delta L/c$ where c is the speed of light. From the slope, we calculate $\Delta L = 0.3$ m, which is approximately the length of a 12-in coaxial cable.

B. For Both Modes, There Is a Constant, π-Phase Difference Between the Resonances Measured at Positive and Negative Biasing Magnetic Field

This is caused by the reversal of the Larmor precession chirality as the biasing magnetic field reverses. For the geometry indicated in Fig. 4(c), the phase lag φ_M between the precessing magnetization $\mathbf{M}$ and the microwave field $h_{\rm RF}$ maintains the same value at the same resonance condition (amplitude of H_B and ω). However, because of the reversed H_B, the precession axis is also reversed, resulting in the opposite polar component M_y. This causes the sign-flip of the instantaneous Kerr signal, and therefore, an additional phase of π introduced in the rectified optical signal. Fig. 5(a) and (b) shows the phase difference between positive and negative resonance fields $\Delta\phi = \phi(+H_B) - \phi(-H_B)$ for the saturated and unsaturated modes, respectively. The deviations from π, -0.08 ± 0.15 rads for Fig. 5(a) and 0.07 ± 0.29 rads for Fig. 5(b), are negligible and within the experimental errorbars.

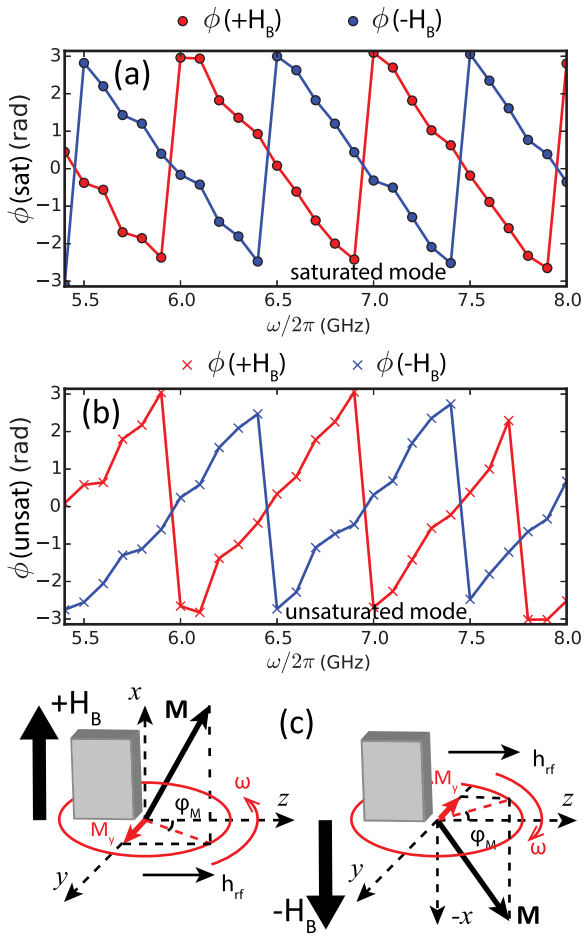

Fig. 4. (a) and (b) Evolution of the extracted ϕ as a function of frequency (5.4–8.0 GHz) for (a) saturated and (b) unsaturated modes, respectively. The notations of ϕ(sat), ϕ(unsat), $\phi(+H_B)$, and $\phi(-H_B)$ are labeled accordingly. (c) Schematics of the macrospin precession and reversed M_y for positive and negative H_B. y-axis: out-of-plane direction. x-axis: directions of H_B. z-axis: direction of $h_{\rm RF}$.

C. Saturated and Unsaturated Modes Have the Opposite ϕ

This observation reflects the most important distinction of the unsaturated mode from the saturated mode. In the unsaturated regime, the total "effective field" applying to the magnetization vector increases as the H_B decreases, and the Kittel equation along the hard axis can be written as [16], [17]

$$\frac{\omega^2}{\gamma^2} = H_y \times H_z \tag{2}$$

where the two effective fields are

$$H_y = H_B\cos\theta_M + M_s + \frac{K_4}{2M_s}(3 - \cos 4\theta_M) \tag{3}$$

$$H_z = H_B\cos\theta_M - \frac{2K_4}{M_s}\cos 4\theta_M. \tag{4}$$

Here, K_4 is the fourfold magnetocrystalline anisotropy coefficient and M_s is the saturation magnetization. θ_M is the angle between M_s and the hard axis (H_B in our case). The uniaxial anisotropy is omitted for simplicity. For our experiments with low H_B values, $H_y(H_B) \approx M_s$. With the approximation,

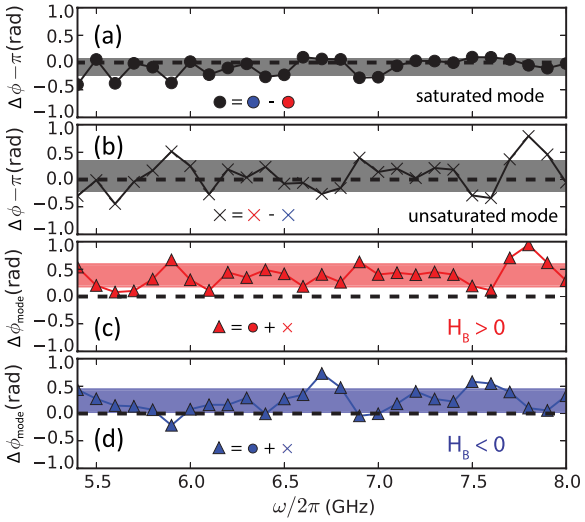

Fig. 5. (a) and (b) Phase shift $\Delta\phi = \phi(+) - \phi(-)$ between the positive and negative resonances for (a) saturated modes and (b) unsaturated modes at 5.4–8.0 GHz. (c) and (d) Mode phase accumulation $\Delta\phi_{\text{mode}} = \phi(\text{sat}) + \phi(\text{unsat})$ between the saturated and unsaturated modes for (c) positive and (d) negative H_B.

the susceptibility of the out-of-plane magnetization M_y around FMR condition is proportional to

$$\frac{\tilde{M}_y}{\tilde{h}_{\text{RF}}} \sim \frac{1}{H_y(H_B)H_z(H_B) - (\omega/\gamma)^2 + i\alpha(\omega/\gamma)(H_y + H_z)} \approx \frac{1}{M_s} \times \frac{1}{H_z(H_B) - (\omega^2/\gamma^2)/M_s + i\alpha\omega/\gamma}. \quad (5)$$

Applying Eq. (2) to Fig. 3 with constant Hy, we find that for the unsaturated modes, H_z has a negative dependence on H_B. This can be also deduced in (4) that as $H_B < 2K_4/M_s$, θ_M evolves from zero to $\pi/4$ and the $\cos 4\theta_M$ term quickly decreases from $+1$ to -1. In this case, Eq. (5) yields a phase change of $+\pi$ instead of $-\pi$ as H_B evolves from below to above the resonance field. In Eq. (1), the extracted ϕ will reverse its sign

$$\phi(\text{unsat}) = -\phi(\text{sat}). \quad (6)$$

To compare with the macrospin model, the mode phase accumulation $\Delta\phi_{\text{mode}} = \phi(\text{sat}) + \phi(\text{unsat})$ is plotted in Fig. 5(d)–(e) using the data from Fig. 4(a) and (b). Surprisingly, we obtain nonzero $\Delta\phi_{\text{mode}}$ as 0.39 ± 0.20 rads for positive H_B and 0.23 ± 0.20 rads for negative H_B. We highlight that the deviation of $\Delta\phi_{\text{mode}}$ from zero are distinct from the strict agreement of $\Delta\phi$ to π shown in Fig. 5(a) and (b). In particular, the saturated mode slightly advances with respect to the unsaturated mode, which is similar to the phase offset reported in X-ray magnetic circular dichroism experiments by Bailey, *et al.* [18]. In their paper, which measured magnetic trilayers with the same flip-chip FMR geometry, a phase advance of 0.6–0.7 rad is identified for the bottom layer with respect to the top layer which is separated by 25 nm. In our case with a single 10 nm FeCo layer, the phase delay of the unsaturated mode may indicate that its magnetization excitation primarily occurs near the top of the film (away from the substrate) due to surface pinning at the FeCo/MgO interface, because the MgO/bcc-FeCo interface usually exhibits large perpendicular anisotropy energy [19]. This finite phase delay should be absent if the top and bottom interfaces of the FeCo film are symmetric. We also note the experimental simplicity of our optical magneto-optic Kerr effect (MOKE) detection compared with the synchrotron-based X-ray measurement in obtaining such phase information.

We also comment that the optical method might make it the only viable method to investigate the microscopic spin precession at the low-field, unsaturated regime, particularly for samples with non-trivial magnetocrystalline anisotropy. First, conventional inductive FMR measurements do not have such phase-resolving capability. Second, spin-torque FMR, which intermixes spin dynamics with the RF electric current, requires the spin rectification effect, i.e., typically the anisotropic-magnetoresistance (AMR) in ferromagnetic metals, to function [20]. However, it has been shown lately that the AMR effect in FeCo is negligible along the hard axis [15], which makes the spin-rectification signal too weak to be convincingly detected for this purpose. Finally, the optical method also allows spatially resolved FMR to be detected in both flip-chip-based continuous films and spin-torque-based nano-devices, which are closely relevant to epitaxial samples with higher order symmetry spin axes, and can be easily integrated in many practical engineering FMR devices [21].

IV. Conclusion

By using a phased-resolved, optically detected FMR technique, we study the evolution of the FMR precessional phase with the excitation frequency across the transition regime between the saturated and unsaturated resonance modes in epitaxial FeCo films. The frequency-dependent precessing phase evolution can be described by a macrospin model in general. However, for the unsaturated modes, we observe a small but non-zero phase offset from the saturated modes. This observation can be interpreted as different spatial mode profiles along the thickness direction due to surface pinning effect. Finally, the optical method has the advantage of resolving both the spatial and phase information in FMR, which makes it suitable for studying FMR of epitaxial magnetic thin film samples with multiple, degenerated spin axes [22]. It can be readily adopted to the investigations of sophisticated magnetic multilayers and nanostructures such as antiferromagnets [23], magnetic phase transitions [24], interface spin-transfer torques [25], spin-torque oscillators [26], artificial spin-ice [27], and topological materials [28].

Acknowledgment

W. Zhang would like to thank Oakland University Startup Funds for equipment acquisition and measurement setup construction. He would also like to thank many helpful discussions with Dr. X. Song and Prof. V. Sih at the University of Michigan.

This work was supported in part by the U.S. National Science Foundation under Grant DMR-1808892, in part by the Michigan Space Grant Consortium, in part by the U.S. Department of Energy, Office of Science, Materials Science and Engineering Division, Argonne, including

coplanar-waveguide preparation and data analysis, in part by the National Key Basic Research Program of China under Grant 2015CB921401, and in part by the National Natural Science Foundation of China under Grant 11474066 and Grant 11734006, Fudan, including sample synthesis and fabrication.

REFERENCES

[1] G. Yu *et al.*, "Switching of perpendicular magnetization by spin–orbit torques in the absence of external magnetic fields," *Nature Nanotechnol.*, vol. 9, pp. 548–554, May 2014.

[2] W. Zhang and K. M. Krishnan, "Epitaxial exchange-bias systems: From fundamentals to future spin-orbitronics," *Mater. Sci. Eng. R, Rep.*, vol. 105, pp. 1–20, Jul. 2016.

[3] Y. Huo, L. H. Bai, P. Hyde, Y. Z. Wu, and C.-M. Hu, "Spin rectification for collinear and noncollinear magnetization and external magnetic field configurations," *Phys. Rev. B, Condens. Matter*, vol. 91, p. 174430, May 2015.

[4] W. Zhang and K. M. Krishnan, "Spin-flop coupling and rearrangement of bulk antiferromagnetic spins in epitaxial exchange-biased Fe/MnPd/Fe/IrMn multilayers," *Phys. Rev. B, Condens. Matter*, vol. 86, p. 054415, Aug. 2012.

[5] W. Zhang and K. M. Krishnan, "Field and temperature-driven magnetic reversal of spin-flop coupled epitaxial Fe/MnPd bilayers," *Phys. Rev. B, Condens. Matter*, vol. 88, p. 024428, Jul. 2013,

[6] W. Zhang, M. E. Bowden, and K. M. Krishnan, "Competing effects of magnetocrystalline anisotropy and exchange bias in epitaxial Fe/IrMn bilayers," *Appl. Phys. Lett.*, vol. 98, no. 9, p. 092503, 2011,

[7] W. Zhang and K. M. Krishnan, "Probing the magnetization reversal in epitaxial Fe/IrMn exchange biased bilayers using angle-dependent anisotropic magnetoresistance," *J. Appl. Phys.*, vol. 111, no. 7, p. 07D712, 2012,

[8] W. Zhang and K. M. Krishnan, "Domain wall nucleation in epitaxial exchange-biased Fe/IrMn bilayers with highly misaligned anisotropies," *J. Magn. Magn. Mater.*, vol. 324, no. 19, pp. 3129–3132, 2012.

[9] K. Sekiguchi *et al.*, "Spin-wave propagation in cubic anisotropic materials," *NPG Asia Mater.*, vol. 9, p. e392, Jun. 2017.

[10] G. A. Prinz, G. T. Rado, and J. J. Krebs, "Magnetic properties of single-crystal {110} iron films grown on GaAs by molecular beam epitaxy (invited)," *J. Appl. Phys.*, vol. 53, no. 3, p. 2087, 1982.

[11] M. T. Johnson, P. J. H. Bloemen, F. J. A. den Broeder, and J. J. de Vries, "Magnetic anisotropy in metallic multilayers," *Rep. Prog. Phys.*, vol. 59, no. 11, p. 1409, 1996.

[12] S. Yoon, J. Liu, and R. D. McMichael, "Phase-resolved ferromagnetic resonance using a heterodyne detection method," *Phys. Rev. B, Condens. Matter*, vol. 93, p. 144423, Apr. 2016.

[13] *THATec Innovation GmbH*. [Online]. Available: https://www.thatec-innovation.com

[14] K. Shikada, M. Ohtake, F. Kirino, and M. Futamoto, "Microstructure and magnetic properties of FeCo epitaxial thin films grown on MgO single-crystal substrates," *J. Appl. Phys.*, vol. 105, no. 7, p. 07C303, 2009.

[15] Y. Li *et al.* "Giant anisotropy of Gilbert damping in epitaxial CoFe films." [Online]. Available: https://arxiv.org/abs/1901.01941

[16] M. Farle, "Ferromagnetic resonance of ultrathin metallic layers," *Rep. Prog. Phys.*, vol. 61, no. 7, p. 755, 1998.

[17] X. Liu, Y. Sasaki, and J. K. Furdyna, "Ferromagnetic resonance in $Ga_{1-x}Mn_xAs$: Effects of magnetic anisotropy," *Phys. Rev. B, Condens. Matter*, vol. 67, p. 205204, May 2003.

[18] W. E. Bailey *et al.*, "Detection of microwave phase variation in nanometre-scale magnetic heterostructures," *Nature Commun.*, vol. 4, p. 2025, Jul. 2013.

[19] S. Peng *et al.*, "Giant interfacial perpendicular magnetic anisotropy in MgO/CoFe/capping layer structures," *Appl. Phys. Lett.*, vol. 110, no. 7, p. 072403, Feb. 2017.

[20] L. Bai *et al.*, "Universal method for separating spin pumping from spin rectification voltage of ferromagnetic resonance," *Phys. Rev. Lett.*, vol. 111, no. 21, p. 217602, 2013.

[21] M. Guan *et al.*, "Ionic modulation of the interfacial magnetism in a bilayer system comprising a heavy metal and a magnetic insulator for voltage-tunable spintronic devices," *Adv. Mater.*, vol. 30, p. 1802902, Aug. 2018.

[22] C. Guillemard, S. Petit-Watelot, S. Andrieu, and J.-C. Rojas-Sánchez, "Charge-spin current conversion in high quality epitaxial Fe/Pt systems: Isotropic spin Hall angle along different in-plane crystalline directions," *Appl. Phys. Lett.*, vol. 113, no. 26, p. 262404, 2018.

[23] W. Zhang *et al.*, "Spin Hall effects in metallic antiferromagnets," *Phys. Rev. Lett.*, vol. 113, no. 19, p. 196602, 2014.

[24] J. Sklenar *et al.*, "Field-induced phase coexistence in an artificial spin ice," *Nature Phys.*, vol. 15, pp. 191–195, Dec. 2018, doi: 10.1038/s41567-018-0348-9.

[25] S. Emori *et al.*, "Interfacial spin-orbit torque without bulk spin-orbit coupling," *Phys. Rev. B, Condens. Matter*, vol. 93, no. 18, p. 180402, 2016.

[26] Y. Li *et al.*, "Probing phase coupling between two spin-torque nano-oscillators with an external source," *Phys. Rev. Lett.*, vol. 118, no. 24, p. 247202, 2017.

[27] M. B. Jungfleisch *et al.*, "High-frequency dynamics modulated by collective magnetization reversal in artificial spin ice," *Phys. Rev. Appl.*, vol. 8, no. 6, p. 064026, 2017.

[28] W. Jiang, G. Chen, K. Liu, J. Zang, S. G. E. te Velthuis, and A. Hoffmann, "Skyrmions in magnetic multilayers," *Phys. Rep.*, vol. 704, pp. 1–49, Aug. 2017.